Intrinsic deviations in fluorescence yield detected x-ray absorption spectroscopy: The case of the transition metal L edges.

Reshmi Kurian[*,1], Kristjan Kunnus[2], Philippe Wernet[2], Sergei M. Butorin[3], Pieter Glatzel[4] and Frank M.F. de Groot[*,1]

[1]Inorganic Chemistry & Catalysis, Debye Institute for Nanomaterials Science, Utrecht University, Universiteitsweg 99, 3584 CG, The Netherlands.

[2] Helmholtz-Zentrum Berlin für Materialien und Energie GmbH, Albert-Einstein-Str. 15, 12489 Berlin, Germany.

[3] Department of Physics and Astronomy, Uppsala University, Box 516, S-751 20 Uppsala, Sweden

[4] European Synchrotron Radiation Facility, Boite Postale 220, 38043 Grenoble Cedex 9,France.

*Reshmi Kurian and Frank M.F. de Groot
R.Kurian@uu.nl & F.M.F.deGroot@uu.nl
Tel: +(31) 30 253 7400
Fax: +(31) 30 251 1027

Abstract

Fluorescence yield (FY) detected x-ray absorption spectrum spectra (XAS) of 3d transition metal ions are calculated from the integrated 2p3d resonant x-ray emission spectrum. The resulting FY-XAS spectra are compared with the normal XAS spectra corresponding to the absorption cross section and significant deviations between both spectra are found. This implies that the assumption that the FY-XAS spectrum identifies with the XAS spectrum is disproved. Especially for the early transition metal systems the differences between FY-XAS and XAS are large, due to the opening of inelastic decay channels from selected x-ray absorption final states. The theoretical calculations show that the difference between FY detection and XAS is largest for the detection in depolarized geometry. The calculations are compared with experimental spectra for oxides and coordination compounds for Fe^{2+}, Co^{2+} and Ni^{2+} systems. The implications for the sum rules in XAS and magnetic circular dichroism experiments are discussed.

I. Introduction

The 2p x-ray absorption spectra ($L_{2,3}$ edges) of 3d transition metal systems are generally measured with electron yield (EY) and fluorescence yield (FY) measurements detection[1]. Transmission measurements are less often applied because the strong absorption cross sections imply the need of a uniform sample thickness below in the order of 1 micron[2, 3]. Only Often x-ray microscopy experiments regularly make use of transmission experiments mode[4, 5] and since the first application of transmission mode XAS to water by Yang and Kirz in 1985[6] approaches have been developed recently for transmission mode detected XAS of water and aqueous solution[7-13]. Still, most 2p XAS experiments are performed with EY measurements, that use drain current, total electron yield detectors (i.e. channeltrons) or the integrated photoemission spectrum. The EY measurements can suffer from surface induced effects, they need vacuum or low-pressure conditions, and they can be affected by electric and magnetic fields[14] and they can suffer from saturation[15]. The alternative detection scheme is with FY. Self-absorption effects in FY yield detection may result in strongly distorted spectral intensities. Dilute systems can ideally be measured with FY and concentrated systems can sometimes be diluted and/or corrected for saturation effects.

It has been shown that FY spectra differ from the x-ray absorption cross section or "true XAS spectra" not only due to saturation effects and self-absorption, but also due to the intrinsic processes of the FY decay. In 1994 it was shown that the FY detected spectrum of a nickel-cyanide complex does not relate to the 2p x-ray absorption XAS spectrum due to the state dependent intensity fluctuations of the fluorescence decay channels[16]. The same mechanism is responsible for the difference between FY-XAS and XAS at the M_5-edge of rare earth systems[17]. In contrast, most experimental studies involving experimental FY spectra do not seem affected by distortions from the XAS spectral shape, or at least they are not analyzed for the possibility as being distorted. To shed some more light on this situation, we carried out a systematic investigation on transition metal spectra for typical systems ranging from $3d^1$ to $3d^9$ ionic ground states.

We use a theoretical approach according to which the FY signal is dominated by the 2p3d resonant x-ray emission spectroscopy (RXES) channels, and calculate the integrated 2p3d RXES spectral shape. Effectively, this can be approximated as the convolution of 2p XAS and 2p3d XES, slightly modified for interference effects. We show that FY detected XAS spectra contain intrinsic deviations from the x-ray absorption cross section in case of the L edges of 3d transition metal systems. The reason for these deviations is found to be the state dependence of the fluorescence channels.

A core hole decays via fluorescence decay and via Auger decay. We define the state dependent decay constants as respectively $k_{FY}(\Gamma)$ and $k_{AUG}(\Gamma)$. Each 2p core hole state Γ has its specific energy, which implies that the state dependent decay also gives an energy dependent decay. The exact energy dependence is modified by the respective lifetime broadenings and interference effects. The total decay rate for the total number of core holes (N), assuming that the decay channels are independent, is given as:

$$\frac{dN(\Gamma,t)}{dt} = -N(\Gamma,t)\left(k_{FY}(\Gamma) + k_{AUG}(\Gamma)\right)$$

In case of the L edges of 3d transition metals, the core hole decays mainly via Auger decay with k_{AUG} being 100 times larger than $k_{FY}(\Gamma)$. In addition, the combined Auger channels can be considered as constant, as has been shown in detail for Ni^{2+}[16]. We can now define the intensity of the fluorescence decay in terms of the decay constants:

$$I_{FY}(\Gamma) \propto \frac{k_{FY}(\Gamma)}{k_{AUG}(\Gamma) + k_{FY}(\Gamma)} \cong \frac{k_{FY}(\Gamma)}{k_{AUG}}$$

Note that if the core hole would decay mainly via fluorescence yield and all fluorescence is detected in the experiment, this equation would yield an, approximately, state independent constant fluorescence yield intensity. The fluorescence yield decay constant is in this work calculated as the integral over the 2p3d x-ray emission channel, which we will show to be strongly state dependent. In contrast, the integrated 2p3s x-ray emission decay is not state dependent, implying that the 2p3s partial FY signal would yield an energy-independent decay intensity, in other words it would yield a signal proportional to the XAS cross section.

In this paper we systematically study the deviations in the FY spectra of the following transition metal systems:

a) Octahedral symmetry with a cubic crystal field splitting (10Dq) of 1.2 eV and the atomic 3d spin-orbit coupling, corresponding to typical divalent oxide systems
b) Octahedral sytmmetry with the 3d spin-orbit coupling set to zero.
c) Low-spin octahedral symmetry for $3d^4$, $3d^5$, $3d^6$ and $3d^7$ systems.
d) Comparison with experimental spectra for $3d^6$, $3d^7$ and $3d^8$ systems

In addition we will study the effect of the inclusion of coherence between the 2p XAS and the 2p3d XES transitions and the polarization effect on the FY spectra.

II. Experiment and theory

a. Computational Details

We have applied crystal-field multiplet theory to calculate the 2p XAS ($L_{2,3}$ edge) spectra and 2p3d RXES spectral shapes. The 2p XAS spectra have been calculated as the dipole transitions from $3d^N$ to $2p^53d^{N+1}$ configurations. The simulations are carried out with the crystal field multiplet approach developed by Thole *et. al* [18, 19]. The atomic values of the Slater integrals are

used, which we calculate by scaling the Hartree-Fock calculated values by 0.8. Because we intend to use a simple model that explains the main features of FY detection, charge transfer effects have been neglected. The 2p3d RXES calculations involve the transition from the $3d^N$ ground state to the $3d^N$ final states through the $2p^5 3d^{N+1}$ intermediate states. This transition is theoretically described by the Kramers-Heisenberg formula [14, 20, 21] and the corresponding matrices involved are the $3d^N$ to $2p^5 3d^{N+1}$ dipole transition coupled to the (identical) $2p^5 3d^{N+1}$ to $3d^N$ dipole decay matrices. The scattering intensity F is given as a function of incident (Ω) and emitted x-ray energy (ω) is given as:

$$F(\Omega,\omega) = \sum_j \left| \sum_i \frac{< 3d^N \mid T_2 \mid 2p^5 3d^{N+1} >< 2p^5 3d^{N+1} \mid T_1 \mid 3d^N[\Psi_0] >}{E_{3d^N} + \Omega - E_{2p^5 3d^{N+1}} + i\Gamma_{2p^5 3d^{N+1}}} \right|^2 \delta(E_{3d^N[\Psi_0]} + \Omega - E_{3d^7} - \omega)$$

The $3d^N$ ground state, $2p^5 3d^{N+1}$ intermediate state and $3d^N$ final state energies (E) are given. Ω and ω are the energies of the incident and emitted photon, respectively, and Γ indicates the lifetime broadening of the intermediate state. T_1 and T_2 indicate the dipole operators for absorption and emission. All calculations have been performed in C_4 symmetry, yielding nine polarization combinations of the left, right and z-polarised x-rays. Using a correlation function description, a full RXES calculation involves potential different polarizations for the absorption and emission step, implying $3^4 = 81$ polarization combinations [22]. We have chosen to assume a fixed polarization for the absorption and also for the emission step, which limits the 81 combinations to the 9 combinations that we have treated. The transition lines have been convoluted using a Lorentzian and Gaussian function to account for the core-hole life time and instrumental resolution respectively. The half width at half maximum of the Lorentzian used are 0.2 eV for the $2p^5 3d^{N+1}$ intermediate state and 0.2 eV for the $3d^N$ final state. The intermediate state lifetime broadening of 0.2 eV is the average value of a typical L_3 edge of a transition metal oxide. The final state lifetime broadening is less known and could be lower than the value of 0.2 eV that we use. We use a Gaussian broadening of 0.2 eV to simulate an 200 meV resolution monochromator, realizing that many actual beamlines have better resolution.

b. Experiment

The data for $LiFePO_4$ [23, 24] and Co_2SiO_4 [24] were measured at beamline I-511, MAX-lab, Lund, Sweden. The total electron yield spectra were recorded in drain-current mode at 90 degrees radiation incidence angle to the surface of the samples while total fluorescence yield was detected with help of the multichannel plate detector at 45 degrees outgoing photon angle (in the horizontal plane) and with help of a diode at ~80 degrees outgoing angle to the surface (in the vertical plane). This experimental set-up prevents self-absorption effects. Samples were in powder form on conducting carbon tape. The experimental on $Cs[NiCr(CN)_6].2H_2O$ has been digitised from reference [16].

III. Results and Discussion:

a. The XAS and FY-XAS of transition metal ions

The comparison between the XAS and FY-XAS for the 2p XAS spectra of the transition metals are presented in Figure 1. The spectra have been generated as the combination of all nine polarization combinations. Figure 2 will show the effects in case of the most used experimental polarizations. The influence of the 3d spin-orbit coupling on the absorption spectra and the FY-XAS are given in the same Figure. The maximum intensities of XAS and FY-XAS are normalized to unity. The transition metal 2p levels split into $2p_{1/2}$ and $2p_{3/2}$ due to the spin orbit coupling. Therefore, the energy separation between the L_3 and L_2 edges is mainly related to the spin orbit coupling on the core 2p levels of the transition metal ion.. Below we analyse the specific issues of each $3d^N$ ground state.

The $3d^1$ system (Ti^{3+}) are shown in Figure 1a. The $3d^1$ system has an atomic Hund's rule $^2D_{3/2}$ ground state. With a cubic crystal field, the ground state has one occupied t_2g state and its symmetry is $^2T_2$. All ground states with a partly filled t_2g level are strongly affected by the 3d spin-orbit coupling which is clear from the Figure 1a, where the lower (upper) panel shows the result with (without) 3d spin-orbit coupling. The 3d spin-orbit coupling modifies the details of the spectral shape. A discrepancy in the L_3-L_2 intensity ratios for the XAS vs. FY-XAS is seen for both the calculations. The $3d^2$ systems (Ti^{2+}) are shown in Figure 1b. The atomic ground state $^3F_2$ and with a cubic crystal field, the ground state has two occupied t_{2g} electrons, with $^3T_1$ symmetry. This ground state is also strongly affected by the 3d spin-orbit coupling (see Figure 1b). Similar to Ti^{3+}, different peaks in between the L_3 and L_2 edge are seen with 3d spin-orbit coupling. A clear effect is that the L_2 edge gains more intensity in the FY-XAS spectrum compared to XAS.

The $3d^3$ systems (V^{2+}) are shown in Figure 1c. The atomic ground state is $^4F_{3/2}$. Within a cubic crystal field, the ground state has three t_2g electrons and is of $^4A_2$ symmetry, which is not affected by 3d spin-orbit coupling. It is clear from Figure 1c that the FY-XAS intensity of the L_2 edge drastically increases the L_2 edge intensity becomes close the intensity of the L_3 edge. The $3d^4$ systems (Cr^{2+}) is given in Figure 1d. The atomic ground state is $^5D_0$ and in octahedral symmetry the ^5E ground state contains three t_2g spin up electrons and one e_g spin up electron. For large crystal field values the ground state has $^3T_2$ low spin symmetry with all the four electrons (three spin up and one spin down) in the t_{2g} state. Spectra for low-spin ground state are shown in Figure 3a. There is a strong influence of the 3d spin-orbit coupling at both high spin and low spin states, which is evident from Figure 1d and 3a. Similar to V^{2+}, a strong increase in the L_2 edge intensity is seen for the FY-XAS spectra compared to the XAS.

The $3d^5$ systems (Mn^{2+}) are given in Figure 1e. The atomic ground state is $^6S_{5/2}$. Within a cubic crystal field, the high spin ground state has three t_2g spin up electrons and two e_g spin up electrons, with $^6A_1$ ground state symmetry. This A_1 symmetry state is, in first approximation, not affected by the 3d spin-orbit coupling, but due to the interplay with mixing of excited symmetry states a small splitting can occur also for Mn^{2+} systems. The low-spin $3d^5$ systems have five electrons in their t_2g shell (three spin up and two spin down), hence a $^2T_1$ ground state, which is

shown in Figure 3b. This low spin ground state is affected by 3d spin-orbit coupling. The $3d^6$ systems (Fe^{2+}) are given in Figure 1f. The maximum spin state is S=2 with an atomic $^5D_2$ symmetry. Within a cubic crystal field, the ground state has four electrons in the t_{2g} state and two electrons in the e_g state, with a $^5T_2$ symmetry state. The low-spin $3d^6$ systems have all the six electrons in the t_{2g} state and an $^1A_1$ symmetry (see Figure 3c). This $^1A_1$ symmetry state is not affected by the 3d spin-orbit coupling.The $3d^7$ systems (Co^{2+}) are given in Figure 1g. The atomic ground state is $^4F_{9/2}$. Within a cubic crystal field, the ground state has, in addition to its three t_{2g} and two e_g states spin-up electrons, two additional t_2g spin-down electrons, with $^4T_1$ symmetry. Due to the partly filled t_{2g} states, the $3d^7$ systems are sensitive to 3d spin-orbit coupling, which is evident form Figure 1g. The low spin $3d^7$ systems have six t_2g electrons and one e_g electron, with a ^2E symmetry state, which is shown in Figure 3d.

$3d^8$ systems (Ni^{2+}) are given in Figure 1h. The ground state symmetry is $^3F_4$. Within a cubic crystal field, the ground state has six t_2g electrons and two e_g spin-up electrons, with a $^3A_2$ ground state. Therefore, the ground state is always a stable high spin state in octahedral symmetry and it is not affected by 3d spin-orbit coupling. The $3d^9$ systems (Cu^{2+}) are given in Figure 1j. The atomic ground state is $^2D_{5/2}$ atomic. Within an octahedral symmetry, there are six t_2g electrons and three e_g electrons, with a ^2E ground state symmetry. Without the 3d spin-orbit coupling, the L_3-L_2 edge intensity ratio is 2:1 (cf Figure 1j). With 3d spin-orbit coupling the branching ratio defined as the intensity of the L_3 edge divided by the total intensity of the 2p XAS spectrum, is affected. In fact, the branching ratio is a direct measure of the mixing of the $3d_{3/2}$ character into the $3d_{5/2}$ atomic ground state due to crystal field effects.

Comparing all nine calculations in Figure 1, one can make the general observations that the FY-XAS spectra have an increased intensity of the L_2 edge and in addition the states at the higher-end of both the L_3 and the L_2 edge increase in intensity. The states at higher energy on average seem to have more and stronger fluorescent decay channels.The increase of the L_2 edge also implies that the branching ratio is significantly affected in FY-XAS spectra.

b. Polarization dependent effects

In photon-in photon-out experiments, the polarization and scattering angle are important additional degrees of freedom. Depending on the polarization of the used x-rays as well as the scattering angle, different combinations of polarizations of the x-ray absorption and x-ray emission transitions are combined. The results for the $3d^{1-9}$ transition metals for the high spin states are given in Figure 2. In Figure 2, we compare the total FY-XAS spectrum with the two most commonly applied experimental settings for soft x-ray emission experiments, where the angle between the incoming x-ray propagation direction and the outgoing x-rays is set to 90°. The incoming x-rays are polarized either linear parallel (depolarized geometry or linear horizontal; LH) or linear perpendicular (polarized geometry or linear vertical; LV) to the scattering plane. It is interesting to note that the LV polarized spectra are essentially identical to the total polarization averaged spectra. The LH polarized spectra show differences with the LV spectra and the polarization averaged spectra. In general the LH spectra have an increased difference with the XAS spectra, as compared with the polarization averaged FY-XAS spectra:

the peaks of the L_2 edge and the peaks at the high-energy side of the L_3 and L_2 edges are further enhanced in LH polarization.

c. Low-spin systems

Figure 3 shows the calculations for the low-spin systems, using a cubic crystal field strength of 10Dq = 2.4 eV. In octahedral symmetry $3d^3$, $3d^4$, $3d^5$ and $3d^6$ systems contain a high-spin to low-spin transition. The low-spin calculations show a similar trend as the high-spin calculations: (1) An increase of the L_2 edge for Cr^{2+}, Mn^{2+} and Fe^{2+} and (2) a transition intensity increase for the states at the end of the L_2 and L_3 edge. This is for example visible for low-spin Co^{2+} as a decrease of the FY-XAS intensity at the low-energy side of the L_3 edge.

d. The consequences for the sum rules

The intensities of the XAS and FY-XAS spectra as a function of the number of core holes are plotted in Figure 4. The XAS intensities form a straight line, exactly confirming the 2p XAS sum rule: the integrated 2p XAS intensity measures the number of empty 3d states. FY-XAS shows a fluctuating line, indicating the difference in the decay channels of FY-XAS. This implies that the sum rule for the number of holes does not apply for FY measurements. This has also implications for the sum rules as used in x-ray magnetic circular dichroism (XMCD). Also for the FY detected XMCD measurements there will be effects due to the energy dependent fluorescence decay, which will cause systematic deviations for both the XAS and the XMCD spectra. The integrated FY-XAS intensity does not have a well-defined meaning unlike the integrated XAS intensity. Its relative intensity depends mainly on how many and how strong x-ray emission channels the 2p core states have. This is strongly dependent on the specific symmetry, in other words on the 3d count, the crystal field effects and also the charge transfer effects. Figure 3 shows that $3d^1$, $3d^3$ $3d^5$, low-spin $3d^7$, $3d^8$ and $3d^9$ have relatively high FY-XAS integrated intensity, compared with the relatively low FY-XAS intensities of the other 3d counts. For example, the Mn^{2+} system reaches a set of intermediate states that have a larger-than-average integrated x-ray emission decay strength, but it is not evident to explain the trends in this behavior.

e. The effects of interference

The inclusion of interference effect can be crucial in some cases as it can create the excitation and decay of intermediate states overlapping in energy. A calculation on $3d^3$ V^{2+} is performed by including the interference effect and plotted along with the FY-XAS omitting interference effect in Figure 5. From the correlation between two plots, we find that the interference effect is important and is strong at the L_3 edge. If interference effects can be neglected one can use a much simpler calculation for the 2p3d RIXS plane, as the Kramers-Heisenberg relation then simplifies to the multiplication of the XAS spectrum with the XES spectrum. What needs to be considered also when interference is neglected is that each $2p^5 3d^{N+1}$ multiplet state can have a decay channel entirely different from its neighbor state that can be almost degenerate in energy. This implies that also without interference effects one still has to calculate the combination of each specific excitation with its related decay spectrum. A further simplification to the direct multiplication of the XAS spectrum with a fixed XES spectrum is not possible. This is in

contrast to systems where multiplet effects are not important and one can use single particle methods such as density functional theory (DFT) to calculate both the XAS and XES spectra [25, 26].

f. Comparison with experiment

Figure 6 shows the comparison with experiment. We compare the calculations respectively with two bulk oxides $LiFePO_4$ [23] and Co_2SiO_4 [24] and a coordination compound $Cs[NiCr(CN)_6].2H_2O$ [16]. $LiFePO_4$ contains $3d^6$ Fe^{2+}, Co_2SiO_4 contains $3d^7$ Co^{2+} and $Cs[NiCr(CN)_6].2H_2O$ contains $3d^8$ Ni^{2+}. For all systems the transmission or electron yield XAS experiments are compared with FY-XAS experiments. The experimental differences between XAS and FY-XAS agree with the calculations. Figure 6a shows the increased L_2 edge plus the increased intensity at the high energy side of the L_3 edge. Figure 6b show the decrease in intensity at the low energy side of the L_3 edge and Figure 6c shows the same effect. Cr^{3+} data also confirms the difference between FY-XAS and XAS[27].

All experiments confirm the theoretical predictions. This also implies that for all systems the FY-XAS is dominated by the 2p3d XES decay channel. Calculations of the radial matrix elements confirm that the 2p3s XES decay channel is weaker by at least a factor of four for all systems. The 2p3s XES does not show an energy dependence, implying that the overall effect of 2p3d and 2p3s XES decay is slightly less extreme than solely the 2p3d XES that has been calculated. This is confirmed by the experiments that show in most cases a slightly weaker effect than the theoretical calculations. Because the 2p3s XES decay does not show an energy dependence it could be used as a PFY detector channel to reveal directly the XAS spectral shape.

There are two effects that could further affect the calculated FY-XAS results: (1) Super Coster-Kronig (SCK) Auger decay channels and (2) charge transfer effects. SCK Auger involves a decay channel from the L_2 edge to the L_3 with the emission of a ~10 eV electron. This is a relatively strong channel. The SCK L_3 state will subsequently decay via other (cascade) Auger channels, but a fraction will decay via the radiative 2p3d XES channel, adding intensity to FY-XAS signal. Recent experiments that detect complete RIXS planes of Cr^{3+} systems confirm the presence of these SCK Auger plus 2p3d XES cascade channels[27, 28]. The SCK Auger decay has two counterbalancing effects on the FY-XAS intensity: (i) the shortened lifetime of the L_2 states decreases the FY-XAS of the L_2 edge and (ii) the SCK Auger decay followed by 2p3d XES cascade channels increases the FY-XAS of the L_2 edge. In the present calculations we do not include charge transfer effects. Charge transfer states have a different degree of localization and it can be expected that the ratio between radiative and non-radiative channels is modified. This implies that systems with significant charge transfer intensity, in particular involving both ligand-metal and metal-ligand charge transfer in molecular π-systems[29,30], can show modified results. On the other hand, we do not expect significant modifications of the results in case of bulk oxides.

IV. CONCLUSION

The fluorescence yield measurements of x-ray absorption spectra are often used as a measure of the x-ray absorption cross section. In this paper we have shown that the fluorescence yield decay channels of the $L_{2,3}$ edges of the transition metals are distinct from the x-ray absorption cross section, and there is a clear difference between the XAS and FY-XAS spectra in case of the 3d transition metal ions. The results show that FY measurements on transition metal L edges are sensitive to the decay channels and hence cannot be taken as an analogue for the Electron Yield measurements or Transmission measurements. This effect is a result of the opening of a fluorescent decay channels for selected absorption transitions. The integrated results show that the sum rule is not applicable on FY-XAS data, which also implies that FY detected X-MCD data are affected and cannot be directly used in a quantitative way using the sum rules. The same conclusion can be made regarding the branching ratio. The calculations are confirmed by four experimental data sets comparing FY-XAS and XAS detection, which confirm the theoretical predictions.

References

[1] J. Jaklevic, J. A. Kirby, M. P. Klein, A. S. Robertson, G. S. Brown, and P. Eisenberger, *Solid State Commun.* **23**, 679 (1977).

[2] J. Stöhr, *XANES Spectroscopy* (Springer, Berlin, 1992).

[3] C. T. Chen, Y. U. Idzerda, H. J. Lin, N. V. Smith, Meigs. G., Chaban. E., Ho. G.H., Pellegrin. E., and F. Sette, *Phys. Rev. Lett.* **75**, 152 (1995).

[4] E. De Smit, et al., *Nature* **456**, 222 (2008).

[5] A. Erbil, G. S. Cargill III, R. Frahm, and R. F. Boehme, *Phys. Rev. B* **37**, 2450 (1988).

[6] B.X. Yang and J. Kirz, *Phys. Rev. B* **36**, 1361.

[7] S. Schreck, G. Gavrila, C. Weniger, and P. Wernet, *Rev. Sci. Instrum.* **82**, 103101 (2011).

[8] P. Wernet, G. Gavrila, K. Godehusen, C. Weniger, E.T.J. Nibbering, T. Elsaesser, and W. Eberhardt, *Appl. Phys. A* **92**, 511 (2008).

[9] L.A. Naslund, J. Luning, Y. Ufuktepe, H. Ogasawara, P. Wernet, U. Bergmann, L.G.M. Pettersson, and A. Nilsson, *J. Phys. Chem. B* **109**, 13835 (2005).

[10] N. Huse, T.K. Kim, L. Jamula, J.K. McCusker, F.M.F. de Groot, and R. W. Schoenlein, *J. Am. Chem. Soc.* **132**, 6809 (2010).

[11] N. Huse, H. D. Wen, D. Nordlund, E. Szilagyi, D. Daranciang, T. A. Miller, A. Nilsson, R. W. Schoenlein, and A. M. Lindenberg, *Phys. Chem. Chem. Phys.* **11** (2009).

[12] M. Nagasaka, T. Hatsui, T Horigome, Y. Hamamura, and N. Kosugi, *J. Elec. Spec.* **177**, 130 (2010).

[13] R. Seidel, et al., *J. Am. Chem. Soc.* **134**, 1600 (2012).

[14] F. M. F. de Groot and A. Kotani, *Core level spectroscopy of solids* (CRC Press, Boca Raton, 2008).

[15] R. Nakajima, J. Stohr, and Y.U. Idzerda, *Phys. Rev. B.* **59**, 6421 (1999).

[16] F. M. F. de Groot, M. A. Arrio, Ph. Sainctavit, Ch. Cartier, and C. T. Chen, *Solid State Commun.* **92**, 991 (1994).

[17] M. Pompa, A. M. Flank, P. Lagarde, J. C. Rife, I. Stekhin, M. Nakazawa, H. Ogasawara, and A. Kotani, *Phys. Rev. B* **56**, 2267 (1997).

[18] B.T. Thole, G. van der Laan, and P. H. Butler, *Chem. Phys. Lett.* **149**, 295 (1988).

[19] F. M. F. de Groot, J. C. Fuggle, B.T. Thole, and G. A. Sawatzky, *Phys. Rev. B* **42**, 5459 (1990).

[20] H. Kramers and W. Heisenberg, *Z. Phys. A At. Nucl.* **31**, 681 (1925).

[21] F. M. F. de. Groot, *Chem. Rev.* **101**, 1779 (2001).
[22] L. J. P. Ament , M. van Veenendaal, T. P. Devereaux, J. P. Hill, and J. v. d. Brink, *Rev. Mod. Phys.* **83**, 705 (2011).
[23] A. Augustsson, et al., *J. Chem. Phys.* **123**, 184717 (2005).
[24] S. M. Butorin, *(unpublished results)*.
[25] F. M. F. de Groot, S. Pizzini, A. Fontaine, K. Hämäläinen, C. C. Kao, and J. B. Hastings, *Phys. Rev. B* **51**, 1045 (1995).
[26] N.Smolentsev, M. Sikora, A.V. Soldatov, K.O.Kvasnina, and P. Glatzel, *Phys. Rev. B.* **84**, 235113 (2011).
[27] K. Kunnus and P. Wernet, *(unpublished results)* (2012).
[28] M.D. Gotz et al., *J. Phys. Chem. Lett.* 3, 1619 (2012).
[29] R.K. Hocking, E.C. Wasinger, F.M.F. de Groot, K.O. Hodgson, B. Hedman, and E. I. Solomon, *J. Am. Chem. Soc.* **128**, 10442 (2006).
[30] R.K. Hocking, E.C. Wasinger, Y.L. Yan, F.M.F. de Groot, F. A. Walker, J.P. Collman, K.O. Hodgson, B. Hedman, and E.I. Solomon *J. Am. Chem. Soc.* **129**, 113 (2007).

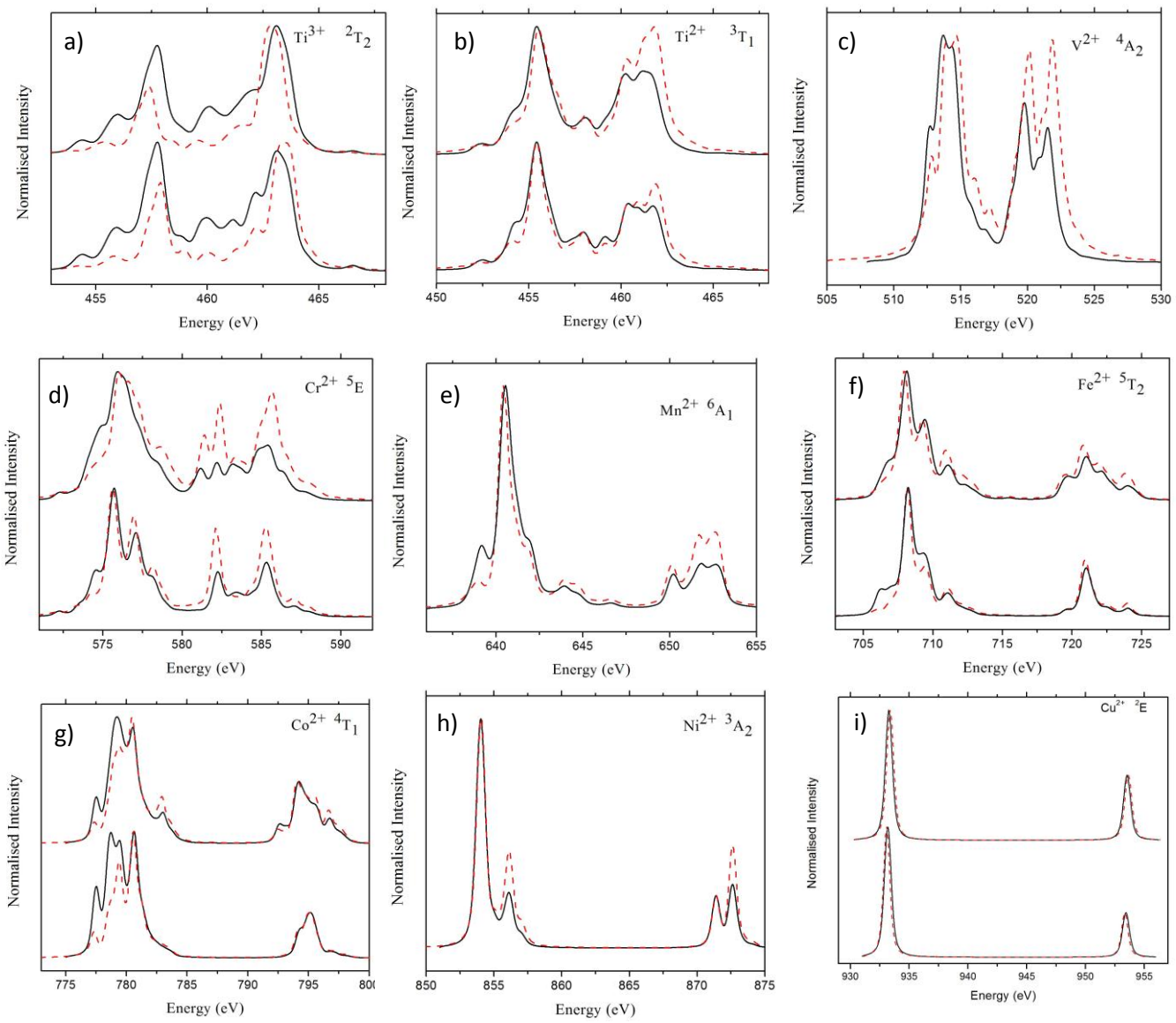

Figure 1: XAS and FY-XAS for the $3d^1$-$3d^9$ transition metal ions with a 10 Dq of 1.2 eV. The lower panel shows the results with 3d spin-orbit coupling and upper panel without 3d spin-orbit coupling. The black solid line shows the XAS and the red dotted line is the FY-XAS spectra.

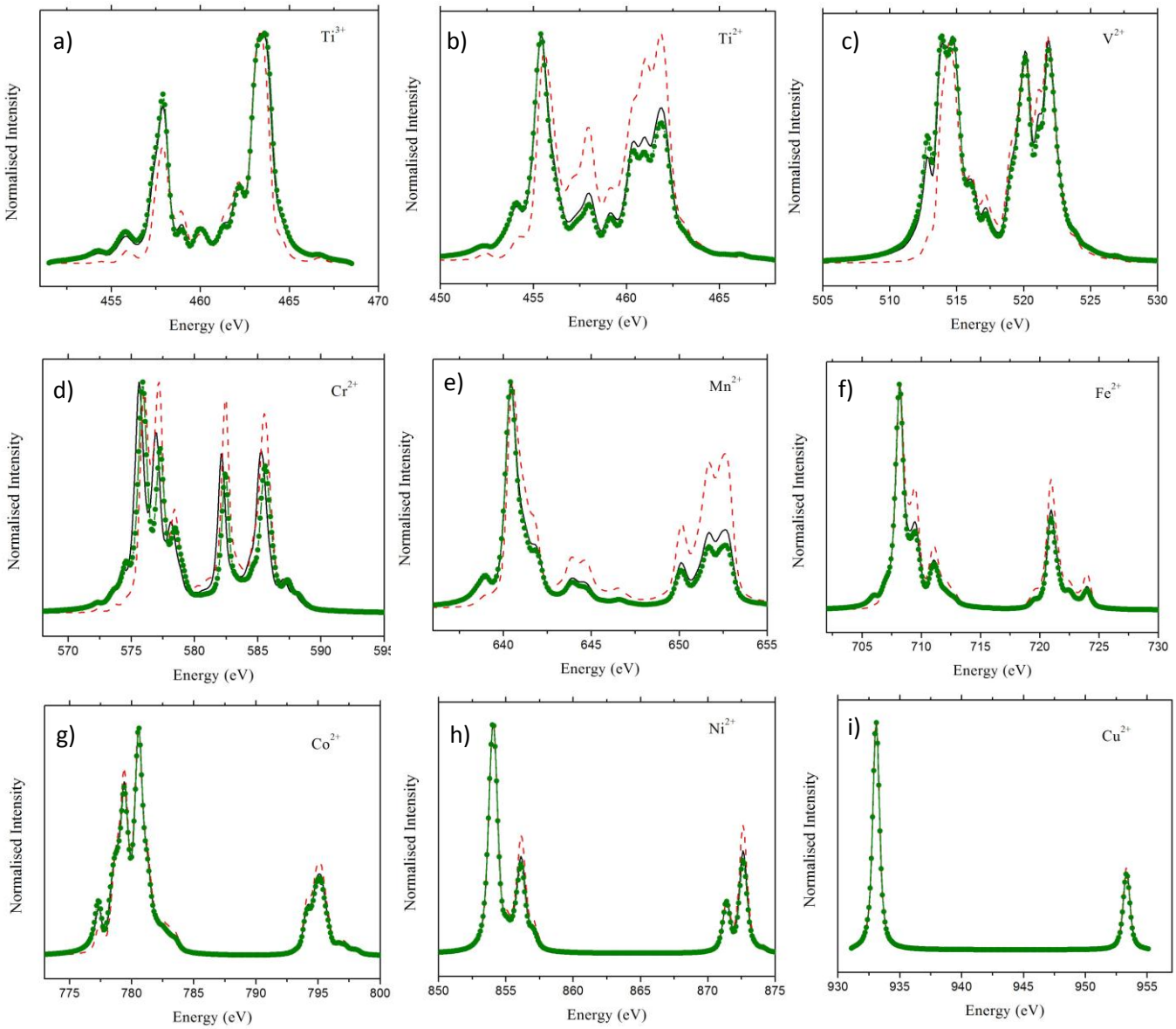

Figure 2: The polarization dependency of the FY-XAS for the $3d^1$-$3d^9$ transition metals is given. The spectra given are FY-XAS (black solid), FY-XAS (LH) (red dashed) and FY-XAS (LV) (green with symbol).

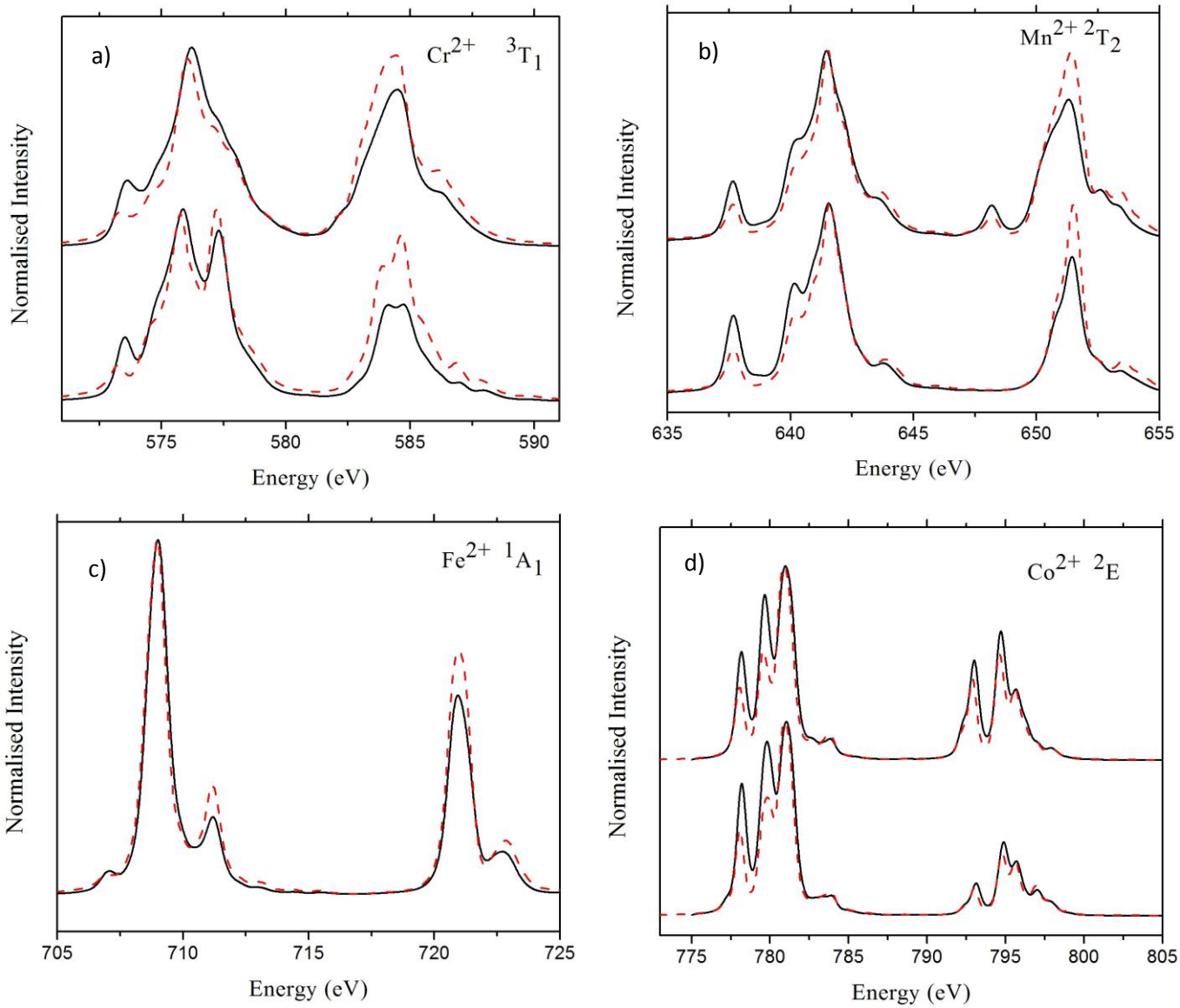

Figure 3: The low spin XAS and FY-XAS spectra for the $3d^4$-d^7 transition metal ions. The lower panel shows the results with 3d spin-orbit coupling and upper panel without 3d spin-orbit coupling. The $^1A_1$ ground state of low-spin Fe^{2+} is not affected by 3d spin-orbit coupling.. The black solid line shows the XAS and the red dotted line is the FY-XAS spectra.

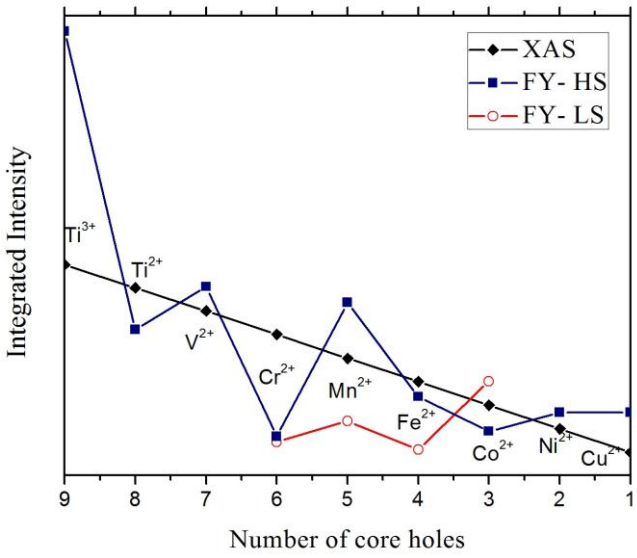

Figure 4: The integrated intensities of the XAS and FY-XAS of $3d^{1-9}$ metals as a function of the number of core holes. The straight line of the XAS results (black), is compared with high-spin (blue) and low-spin (red) FY-XAS calculations.

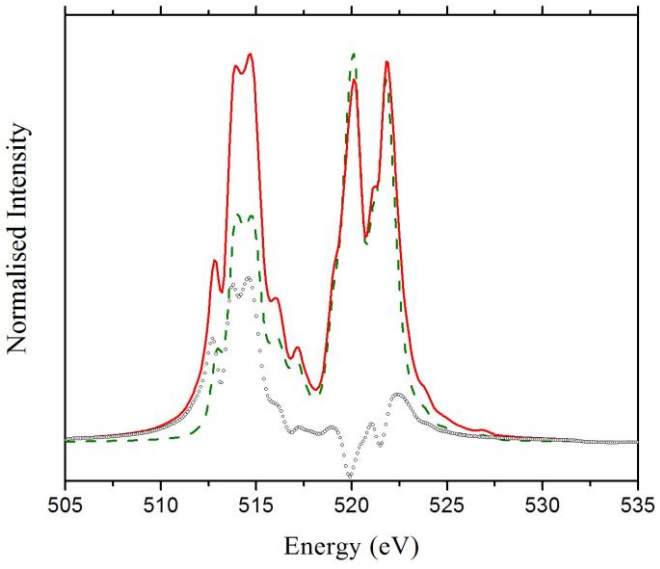

Figure 5: The interference effect on the FY-XAS spectra for $3d^3$ (V^{2+}). The solid (red) line shows the spectra with including the interference effect and the dashed (green) line without it, the difference between both spectra is shown with the dotted (blue) line.

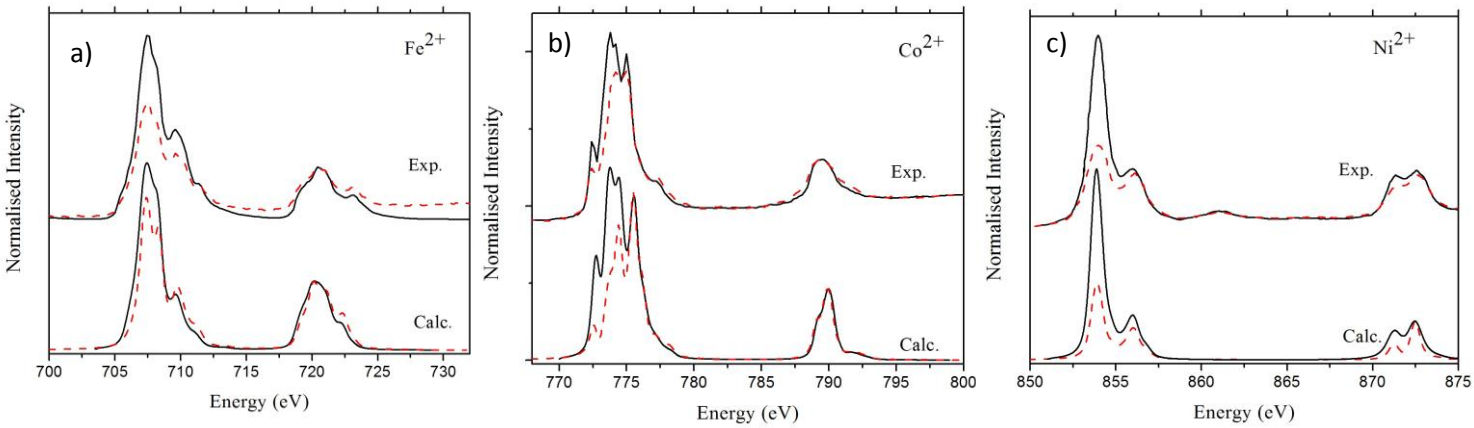

Figure 6: The comparison of the simulated XAS (black, solid line) and FY-XAS (red, dashedline) spectra with the experimental spectra. From left to right respectively a) Fe^{2+}(measured on $LiFePO_4$ [23]), b) Co^{2+} (measured on Co_2SiO_4 [24]) and c) Ni^{2+} (experiment on $Cs[NiCr(CN)_6].2H_2O$ [16]) respectively. The XAS and FY-XAS specrtra are normalized so that the maximum of L_2 edge coincide each other.